frontiers | Frontiers in Physics

TYPE Original Research
PUBLISHED 06 December 2024
DOI 10.3389/fphy.2024.1487954

OPEN ACCESS

EDITED BY
Oscar Moreno,
Complutense University of Madrid, Spain

REVIEWED BY
Chen Ji,
Central China Normal University, China
Francesco Giovanni Celiberto,
University of Alcalá, Spain

*CORRESPONDENCE
Tsunenori Inakura,
inakura@gmail.com
Shuichiro Ebata,
ebata@mail.saitama-u.ac.jp

RECEIVED 29 August 2024
ACCEPTED 05 November 2024
PUBLISHED 06 December 2024

CITATION
Inakura T and Ebata S (2024) Mixing of isoscalar and isovector characteristics in the low-energy dipole mode.
Front. Phys. 12:1487954.
doi: 10.3389/fphy.2024.1487954

Mixing of isoscalar and isovector characteristics in the low-energy dipole mode

Tsunenori Inakura[1,2]* and Shuichiro Ebata[3]*

[1]Office of Institutional Research and Decision Support, Tokyo Institute of Technology, Tokyo, Japan, [2]Laboratory for Zero-Carbon energy, Institute of Innovative Research, Tokyo Institute of Technology, Tokyo, Japan, [3]Graduate School of Science and Engineering, Saitama University, Saitama, Japan

We investigated isospin splitting in low-energy dipole (LED) states of spherical nuclei such as ^{40}Ca, ^{90}Zr, ^{132}Sn, ^{208}Pb, and several $N = 50$ isotones using self-consistent Hartree–Fock plus random phase approximation calculations. Our analysis of isovector dipole (IVD) and isoscalar dipole (ISD) strengths, along with transition densities, reveals a clear energy-dependent relationship between IS and IV modes in ^{40}Ca and ^{90}Zr. For ^{208}Pb and ^{132}Sn, LED states show mixed IS + IV characteristics due to different neutron and proton shell structures. In $N = 50$ isotones, $E1$ modes exhibit varying IS and IV properties with smooth transitions as neutron excess increases. Our results suggest that compressional ISD strengths could provide valuable insights into the slope parameter of the nuclear equation of state. The observed dependence on nuclear shell structures and neutron–proton correlations highlights the need for precise measurements and further research in nuclear physics.

KEYWORDS

electric dipole mode, PDR, isoscalar and isovector characteristics, RPA, energy density functional, Hartree–Fock method

1 Introduction

Low-energy dipole (LED) excitation is one of the key ingredients to investigate nuclear properties. The LED states appear in low excitation energy compared with the excitation energy of giant dipole resonance (GDR), having sizable strengths up to several percentage of the Thomas–Reiche–Kuhn sum rule. They have been observed in wide nuclear mass regions, e.g., ^{48}Ca [1], ^{68}Ni [2], ^{90}Zr [3, 4], ^{132}Sn [5], and ^{208}Pb [6]. The systematic calculations for the dipole mode ($E1$) [7–9] show that the LED state appears in many isotopes. The LED state on a neutron-rich nucleus has been called the pygmy dipole resonance, which is often interpreted as a collective oscillation of the neutron skin and the remnant core [10, 11] (skin-core oscillation). There have been many studies for the LED to probe the properties of neutron matter, nuclear symmetry energy, and the slope parameter in the equation of state of neutron matter. However, its nature is still under debate.

It is found from recent experiments [12–19] that the LED state has two components in its lower- and higher-energy regions. The lower LED has an isoscalar (IS) + isovector (IV) characteristic, whereas the higher LED has IV dominant characteristic. These characteristics are indicated by comparing the $E1$ strengths induced by (α, α') scattering for the IS characteristic and (γ, γ') scattering for the IV characteristic. This phenomenon is called LED isospin splitting. Several theoretical calculations [20–31] using the (quasi-particle) random-phase approximation (RPA) show that the calculated LED state in magic nuclei has both

IS and IV characteristics in its strengths and transition densities. However, the underlying structure of LED isospin splitting is not well-understood yet.

To investigate LED isospin splitting, we systematically study the LED states of several spherical nuclei and $N = 50$ isotones, using the RPA calculation, which describes the IV dipole (IVD) and the compressional IS dipole (ISD) modes. We obtain the pure IS characteristic (and pure IV character) in the $E1$ modes of ^{40}Ca and ^{90}Zr, while the isospin-mixed LED strengths appear in $N \gg Z$ nuclei. Isospin-mixing is induced by proton and neutron shell structures near the Fermi levels. Our calculation for $N = 50$ isotone shows that the $E1$ mode with the pure IS characteristic varies smoothly to the lower component in LED isospin splitting. The LED is expected to be a substitute for observing the slope parameter L of the nuclear equation of state (EOS). There have been many studies to investigate which observable LED has the strongest correlation with L, but we have not yet pinned down the value of L. We show that low-energy compressional ISD strengths might be a suitable probe of L.

The manuscript is organized as follows: Section 2 reviews briefly the Hartree–Fock (HF) and the RPA calculation. In Section 3, we calculate the LED states in ^{40}Ca, ^{90}Zr, ^{208}Pb, and ^{132}Sn and analyze the properties of LED isospin splitting. Changes in the LED properties in $N = 50$ isotones are shown. We mention the relation between the ISD strength and L. Conclusions are given in Section 4.

2 Methods

We employ the HF + RPA approach to describe LED states. The numerical code used in the present calculation is a revised version of the code developed in [32].

We use the Skyrme effective interaction and the minimal nuclear energy density functional (EDF) [33]. The Skyrme interaction is an EDF often used in mean-field model calculations and is characterized by being expanded in terms of delta functions in space. The parameter set is determined according to each protocol. The adopted Skyrme interactions are SkM* [34], SLy4 [35], UNEDF1 [36], SkI2, and SkI3 [37] parameter sets. The minimal EDF has been recently presented as an EDF with the smallest number of possible phenomenological parameters. The SeaLL1 parameter set is used in this work. The pairing correlation is ignored in this paper because its contribution to LEDs is small, as shown in [9]. We only restrict our consideration to spherical nuclei to avoid complicating the discussion with nuclear deformation and pairing effects. Therefore, the HF + RPA approach is a sufficient model for our purpose, when we discuss the LED in closed-shell and spherical nuclei.

Here, two operators for IVD and compressional ISD are introduced to investigate isovector and isoscalar characteristics in LED. The IVD operator $\widehat{D}$ is expressed as

$$\widehat{D} = \frac{N}{A}\sum_{i\in p} r_i Y^{(1)}(\Omega_i) - \frac{Z}{A}\sum_{i\in n} r_i Y^{(1)}(\Omega_i),$$

where $Y^{(1)}$ denotes the spherical harmonics for the dipole mode $\ell = 1$. The index $i \in p$ ($i \in n$) indicates that the sum runs over protons (neutrons). For the compressional ISD mode, the operator,

$$\widehat{D}_{\rm IS} = \sum_{i\in n,p}\left(r_i^2 - \frac{5}{3}\langle r^2\rangle\right) r_i Y^{(1)}(\Omega_i),$$

is adopted where $5\langle r^2\rangle/3$ is introduced to eliminate the center-of-mass contribution.

The $E1$ transition strength from the ground state $|0\rangle$ to the excited state $|\alpha\rangle$ by $\widehat{D}$ or $\widehat{D}_{\rm IS}$ in an even-even nucleus is $B(E1;\alpha) = \left|\langle\alpha|\widehat{D}|0\rangle\right|^2$ or $B({\rm IS}E1;\alpha) = \left|\langle\alpha|\widehat{D}_{\rm IS}|0\rangle\right|^2$. The transition amplitude $\langle\alpha|\widehat{D}|0\rangle$ can be calculated within HF + RPA for the one-particle-one-hole excitations. Using them, the strength function is given by smearing out with the Lorentzian and is written by

$$S(E1,E) = \frac{\gamma}{\pi}\sum_\alpha\left[\frac{1}{(E-E_\alpha)^2+\gamma^2} - \frac{1}{(E+E_\alpha)^2+\gamma^2}\right]\left|\langle\alpha|\widehat{D}|0\rangle\right|^2,$$

where E_α is the energy of the excited state $|\alpha\rangle$ and the strength function is denoted as $S({\rm IS}E1;\alpha)$ for $\widehat{D}_{\rm IS}$. We adopt $2\gamma = 1$ MeV throughout this paper.

The excited states are analyzed by using particle–hole (ph) contribution C_{ph} and transition density $\delta\rho$, which are obtained in the HF + RPA calculations. The ph contribution of an excitation from the i orbit to the m orbit is evaluated, with the forward and backward amplitudes $X_i(\mathrm{r})$ and $Y_i(\mathrm{r})$, as

$$C_{mi} = |X_{im}|^2 - |Y_{im}|^2,$$

in which X_{im} is extracted from $X_i(\mathrm{r})$ as

$$X_{im} = \int d\mathrm{r}\quad \phi_m^*(\mathrm{r})\,X_i(\mathrm{r})$$

and similar for Y_{im}. Here, ϕ_m is the mth wave function and the spin index is omitted for simplicity. The transition density $\delta\rho$ is expressed as

$$\delta\rho(\mathrm{r}) = \sum_{i\in n,p}\left\{\phi_i^*(\mathrm{r})\,X_i(\mathrm{r}) + Y_i^*(\mathrm{r})\,\phi_i(\mathrm{r})\right\}.$$

The radial dipole transition density $\delta\rho_{L=1}(r)$ is calculated from $\delta\rho$ as

$$\delta\rho_{L=1}(r) = \int d\Omega\quad rY^{(1)}(\Omega)\quad \delta\rho(\mathrm{r}).$$

The size of the RPA matrix is reduced by assuming the reflection symmetry of the ground state with respect to $x = 0$, $y = 0$, and $z = 0$ planes. We adopt the three-dimensional coordinate (3D) representation within a sphere of radius $R_{\rm box} = 25$ fm with a uniform mesh spacing of 0.6 fm.

Furthermore, we introduce an index for the isospin structure ($I_{\rm iss}$) of the excited state to quantify the isospin characteristic of the dipole mode. $I_{\rm iss}$ is obtained from the transition densities of the neutron and proton at the state with an excitation energy E as

$$I_{\rm iss}(E) = \frac{\int d\mathrm{r}\quad |Z\delta\rho^\nu(\mathrm{r};E) - N\delta\rho^\pi(\mathrm{r};E)|}{\int d\mathrm{r}\quad |Z\delta\rho^\nu(\mathrm{r};E)| + |N\delta\rho^\pi(\mathrm{r};E)|},$$

where $\delta\rho^{\pi(\nu)}$ denotes the transition density on protons (neutrons). If $I_{\rm iss}(E) \simeq 0$, it means that the transition density has almost the same distributions in both the proton and neutron, and the state with energy E has a pure IS characteristic. On the contrary, if $I_{\rm iss}(E) \simeq 1$, the transition densities are out of phase over the space r, and the state has a pure IV characteristic. Then, $I_{\rm iss}(E)$ with less than or over 0.5 means the state has an IS or IV dominant

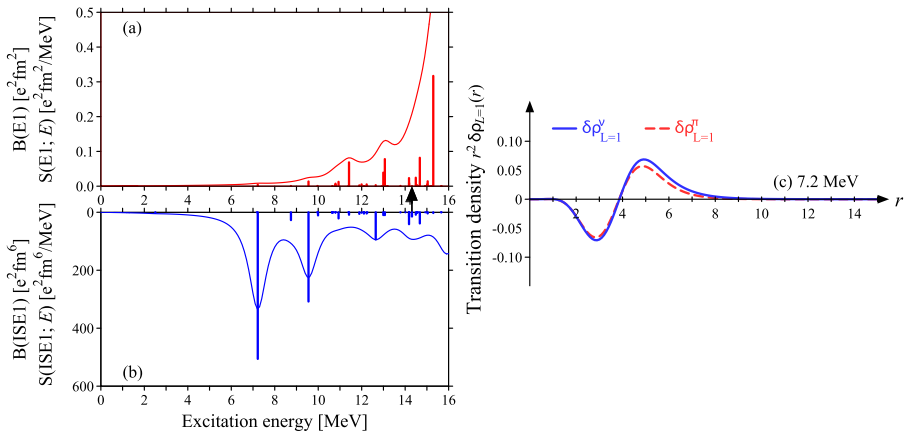

FIGURE 1
IVD and ISD strength and strength functions of ^{40}Ca are shown in **(A, B)**, respectively. The arrow indicates the neutron threshold energy. **(C)** Neutron (solid) and proton (dashed) transition densities $r^2\delta\rho_{L=1}$ of the $E1$ mode at 7.2 MeV.

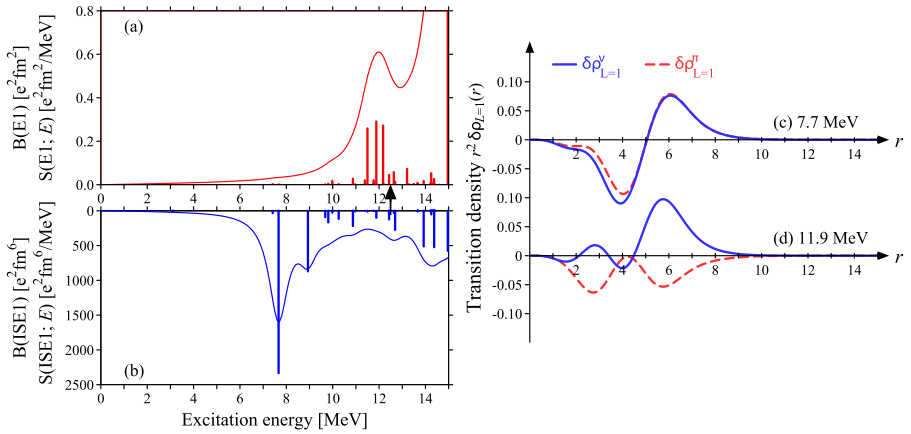

FIGURE 2
Same as Figure 1 but for ^{90}Zr. **(A)** IVD strength, **(B)** ISD strength, **(C, D)** transition densities of the 7.7, and 11.9-MeV states, respectively.

TABLE 1 Calculated ph contributions C_{ph} of LED states in ^{90}Zr.

7.7-MeV state (I_{iss} = 0.030)			
$\nu:1f_{5/2} \to 2d_{5/2}$	0.377	$\pi:2p_{1/2} \to 3s_{1/2}$	0.117
$\nu:2p_{1/2} \to 3s_{1/2}$	0.220	$\pi:1f_{5/2} \to 2d_{5/2}$	0.056
$\nu:1g_{9/2} \to 1h_{11/2}$	0.052	$\pi:1f_{7/2} \to 1g_{9/2}$	0.038
$\nu:1f_{5/2} \to 2d_{3/2}$	0.034	$\pi:1f_{7/2} \to 1g_{7/2}$	0.011
11.9-MeV state (I_{iss} = 0.856)			
$\nu:2p_{3/2} \to 3s_{1/2}$	0.189	$\pi:2p_{3/2} \to 3s_{1/2}$	0.096
$\nu:2p_{3/2} \to 2d_{3/2}$	0.082	$\pi:2p_{3/2} \to 2d_{3/2}$	0.082
$\nu:2p_{3/2} \to 2d_{5/2}$	0.044	$\pi:2p_{3/2} \to 2d_{5/2}$	0.057
$\nu:2p_{1/2} \to 2d_{3/2}$	0.014	$\pi:2p_{1/2} \to 2d_{3/2}$	0.048

characteristic, and the $I_{iss}(E) \sim 0.5$ state has an IS + IV mixed characteristic.

3 Results and discussion

We calculate the E1 strengths and transition densities of the IVD and ISD modes, focusing mainly on their LED states. First, we show the LED modes in ^{40}Ca and ^{90}Zr, which hold isospin symmetry in their excited states. Next, we investigate the LED states in both stable (^{208}Pb) and unstable (^{132}Sn) nuclei, where $N \gg Z$, demonstrating the emergence of isospin mixing in the excited states. We also investigate the interaction dependence of the LED properties for ^{90}Zr and ^{132}Sn. Then, we show how the LED properties change in $N = 50$ isotones: ^{100}Sn, ^{90}Zr, ^{82}Ge, ^{78}Ni, and ^{70}Ca. Finally, we evaluate the relations between the slope parameter L and some quantities of dipole strengths. We can guess that the strength of compressional ISD modes is a more suitable value to probe the slope parameter than the IVD strength, dipole polarization, and partial cross sections of the LED.

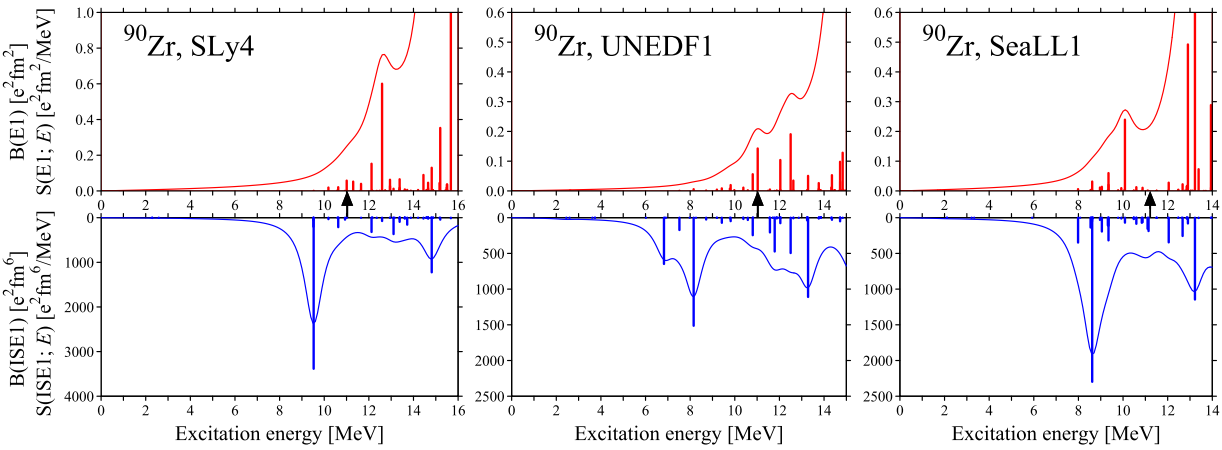

FIGURE 3
IVD and ISD strengths in ^{90}Zr are displayed in upper and lower panels, respectively. The results were obtained using SLy4, UNEDF1, and SeaLL1 parameter sets.

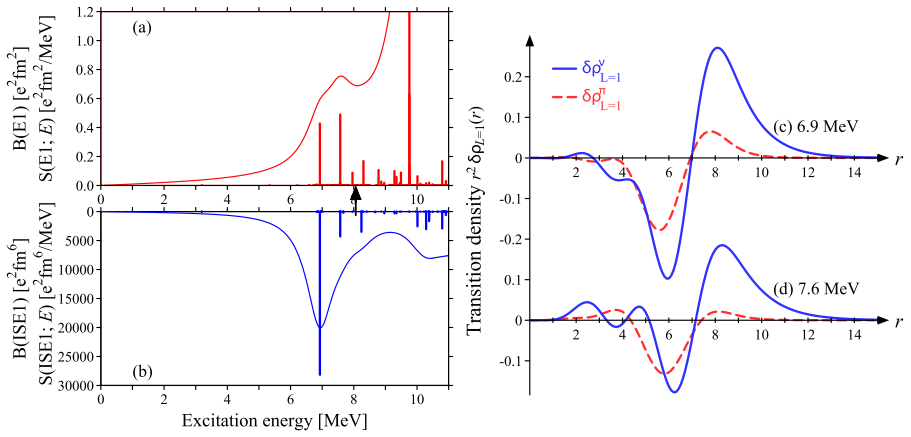

FIGURE 4
Same as Figure 1 but for ^{208}Pb. **(A)** IVD strength, **(B)** ISD strength, **(C)** transition density of the 6.9-MeV state, and **(D)** transition density of the 7.6-MeV state.

3.1 ^{40}Ca and ^{90}Zr

For the $N = Z$ nucleus, ^{40}Ca, Figures 1A, B show the IVD and ISD transition strengths, $B(E1;E)$ and $B(\mathrm{ISE1};E)$, and the strength functions $S(E1;E)$ and $S(\mathrm{ISE1};E)$. They are calculated with the SkM* interaction. The $E1$ mode with a large ISD strength appears at the excitation energy 7.2 MeV, which is the lowest in the LED states, while it has a negligibly small IVD strength. The radial transition densities $r^2\delta\rho_{L=1}$ of the lowest state are plotted in Figure 1C. Proton (π) and neutron (ν) transition densities, $\delta\rho^{\pi}_{L=1}$ and $\delta\rho^{\nu}_{L=1}$, are in phase and almost the same, indicating pure IS characteristic. Its index for isospin structure $I_{\mathrm{iss}} = 0.044$ also signifies the pure IS characteristic. A coherent superposition of proton and neutron excitations π, ν:$1d_{3/2} \rightarrow 2p_{3/2}$ and $1d_{5/2} \rightarrow 1f_{7/2}$ generates the state at 7.2 MeV. This isospin-symmetric mechanism is a characteristic transition on the $E1$ excitation in $N = Z$ nuclei, due to the similar shell structures near the Fermi levels in both the proton and neutron. It should be noted that the low-energy ISD mode is also obtained in another isospin-symmetric $N = Z$ stable nucleus, ^{16}O [21, 31].

Figures 2A, B show $E1$ strengths for ^{90}Zr, same as Figure 1. Similar to ^{40}Ca, the $E1$ state at 7.7 MeV has a large ISD strength and a negligibly small IVD strength. Its transition density is displayed in Figure 2C, which seems to have a pure IS characteristic and indicates $I_{\mathrm{iss}} = 0.030$. The state is generated by coherent superposition of proton and neutron excitations, π, ν: $1f_{5/2} \rightarrow 2d_{5/2}$ and $2p_{1/2} \rightarrow 3s_{1/2}$, as listed in Table 1 where we list large contributions C_{ph} of the decomposed ph excitations. The highest occupied neutron orbit is $1g_{9/2}$, which only contributes to the LED state at 7.7 MeV. The $E1$ transition between $1g_{9/2}$ and $1h_{11/2}$ is the one major shell excitation and a node-less excitation, which needs nodes to be orthogonal to the center-of-mass mode. Then, its contribution C_{ph} gets small, $C_{\mathrm{ph}} = 0.052$ (Table 1). Therefore, although ^{90}Zr has 10 more neutrons than protons, its LED properties are almost the same as those of the $N = Z$ nuclide (^{40}Ca), which has a large ISD strength.

TABLE 2 Calculated ph contribution C_{ph} of LED states in ^{208}Pb.

6.9-MeV state (I_{iss} = 0.237)			
$\nu:2f_{5/2} \to 3d_{5/2}$	0.250	$\pi:1h_{11/2} \to 1i_{13/2}$	0.052
$\nu:1h_{9/2} \to 2g_{9/2}$	0.187	$\pi:1h_{11/2} \to 1i_{11/2}$	0.034
$\nu:1i_{13/2} \to 1j_{15/2}$	0.103	$\pi:2d_{3/2} \to 3p_{3/2}$	0.020
$\nu:3p_{3/2} \to 3d_{5/2}$	0.048	$\pi:1g_{7/2} \to 2f_{7/2}$	0.014
$\nu:2f_{5/2} \to 3d_{3/2}$	0.031	$\pi:3s_{1/2} \to 3p_{3/2}$	0.011
7.6-MeV state (I_{iss} = 0.417)			
$\nu:1h_{9/2} \to 2g_{9/2}$	0.199	$\pi:2d_{5/2} \to 1h_{9/2}$	0.038
$\nu:3p_{3/2} \to 3d_{5/2}$	0.173	$\pi:1h_{11/2} \to 1i_{13/2}$	0.033
$\nu:2f_{5/2} \to 3d_{5/2}$	0.167	$\pi:1h_{11/2} \to 1i_{11/2}$	0.030
$\nu:3p_{3/2} \to 3d_{3/2}$	0.088	$\pi:3s_{1/2} \to 3p_{3/2}$	0.016
$\nu:2f_{5/2} \to 3d_{3/2}$	0.075	$\pi:2d_{5/2} \to 2f_{7/2}$	0.013

The LED states with large IVD and small ISD strengths appear at approximately 12 MeV. Three peaks appear in the IVD strengths, but their transition densities and C_{ph}s are similar to each other. The transition densities of the $E1$ mode at 11.9 MeV are shown in Figure 2D. The aspect of the out-of-phase $\delta\rho^{\nu}$ and $\delta\rho^{\pi}$ indicates a result of the fragmentation of the GDR due to their two bumps. The $E1$ mode has the transition densities of a typical pure IV characteristic, also shown in its I_{iss} = 0.856.

The $E1$ modes with pure IV and IS characteristics with energetic differences appear in the LED strengths of ^{90}Zr. The LED modes with large ISD and small IVD strengths appear in lower energy (at 7.2 MeV), and the LED modes with the opposite $E1$ strength distribution in higher energy (at approximately 12 MeV). This property of strength is consistent with that of LED isospin splitting. Furthermore, similar results can be obtained in other interactions shown in Figure 3. For SLy4, UNEDF1, and SeaLL1 interactions, the lower-LED modes with large ISD and negligibly small IVD strengths appear at ≈ 8 − 10 MeV, and the higher-LED modes with large IVD and small ISD strengths appear around the neutron threshold energy.

The mechanism to induce LED is the same for all interactions in this work. The interaction dependence appears in the strengths and energy position of the LED, which is a result of the chemical potential and nuclear shell structure.

3.2 ^{208}Pb and ^{132}Sn

Here, we show $E1$ strengths and transition densities of LED states in $N \gg Z$ nuclei: ^{208}Pb and ^{132}Sn. Figure 4 shows the $E1$ strengths and transition densities in ^{208}Pb, similar to Figure 1, calculated with the SkM* interaction. The lowest $E1$ mode at 6.9 MeV has both large ISD and IVD strengths, which is clearly different from ^{40}Ca and ^{90}Zr. The second-lowest $E1$ mode appears at 7.6 MeV, with a large IVD strength and small but non-negligible ISD strength. Their transition densities of 6.9 MeV and 7.6 MeV states, displayed in Figures 4C, D, can be interpreted as the skin-core oscillation. This $E1$ mode of ^{208}Pb differs from that of $N = Z$ nuclei, in which protons and neutrons act coherently. The differences come from the nuclear structures near the Fermi levels of nucleons. The $E1$ excitation mode in ^{208}Pb is described by the superposition of neutron (proton) single ph excitations over the $N = 126$ ($Z = 82$) gap. This mechanism makes it difficult to induce purely the in-phase transition densities of neutrons and protons, unlike ^{40}Ca and ^{90}Zr, and causes mixing of the ISD and IVD modes, namely, the IS + IV characteristic in the LED states. The ph contributions of the 6.9 and the 7.6 MeV states, listed in Table 2, are not much different. In both states, significant contributions from four neutron ph excitations, namely, $2f_{5/2} \to 3d_{5/2}$, $1h_{9/2} \to 2g_{9/2}$, $3p_{3/2} \to 3d_{5/2}$, and $2f_{5/2} \to 3d_{3/2}$, exhaust 50% of the total. I_{iss}s of the 6.9 MeV and 7.6 MeV states are 0.237 and 0.417, respectively. Both modes should be interpreted as IS + IV characteristic modes, although the transition densities of the 7.6 MeV state seem to have a dominant IV characteristic trend.

Figure 5 shows the LED states of a neutron-rich unstable nucleus ^{132}Sn which are calculated with the SkM* interaction. Similar to ^{208}Pb, some $E1$ modes appear around the neutron threshold energy with large IVD and ISD strengths. We pick up three $E1$ states with large strengths at 7.2 MeV, 8.0 MeV, and 8.6 MeV. The 7.2-MeV state has the largest ISD strength lower than 10 MeV, and its I_{iss} is 0.237. The 8.0-MeV state has large ISD and IVD strengths and I_{iss} = 0.448, indicating the IS + IV characteristic. The 8.6-MeV state has large IVD and small ISD strengths with I_{iss} = 0.388, which also indicates the IS + IV characteristic. At a glance, three states have the characteristics of IS, IS + IV, and IV dominances in their $E1$ strengths, respectively, but their I_{iss} signify IS + IV characteristics of three modes. To investigate the isospin characteristic of the $E1$ state, not only the strength but also the transition density are necessary. It is not easy to separate pure IS and IV characteristics of the LED modes in $N \gg Z$ nuclei because different proton and neutron shell structures near the Fermi levels hardly induce in-phase transition densities of protons and neutrons, irrespective of the interactions used.

Figure 6 shows the LED strengths calculated with other interactions to compare with them. The LED modes in ^{132}Sn occupy ~2% of the ISD energy-weighted sum rule value, regardless of which interaction is used. We can see similar LED strengths of the SkM* in other interactions, although some detail differences exist, similar to the case of ^{90}Zr. From the $E1$ strength distribution viewpoint, LED isospin splitting is less clear than SkM*in the results using SLy4, UNEDF1, SkI2, SkI3, and SeaLL1 due to large ISD and IVD strengths in the states. These interaction differences in LED isospin splitting are attributed to different structures of single-particle states near the Fermi levels and to the correlation between protons and neutrons, which induces the IS + IV characteristic of the LED modes.

3.3 Transition of LED isospin splitting in N = 50 isotones

The LED strengths and its transition densities for ^{40}Ca, ^{90}Zr, and $N \gg Z$ nuclei are investigated in the above sections. For the

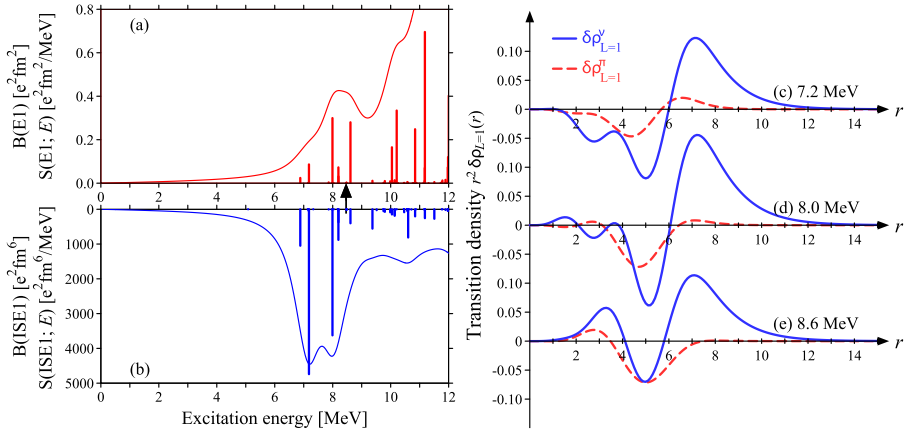

FIGURE 5
Same as Figure 1 but for ^{132}Sn. **(A)** IVD strength, **(B)** ISD strength, **(C–E)** transition densities of the 7.2, 8.0, and 8.6-MeV states, respectively.

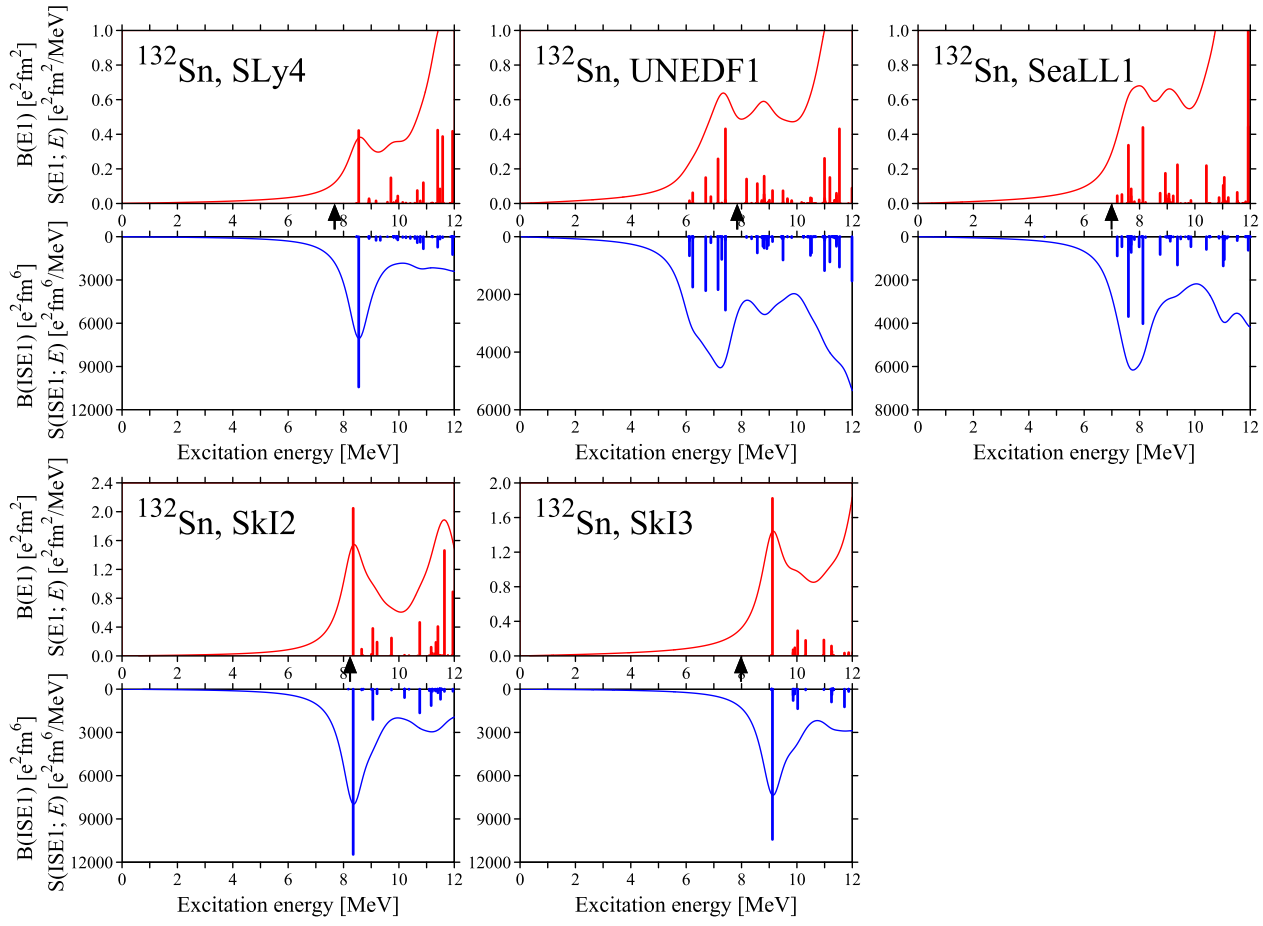

FIGURE 6
Same as Figure 3 but for ^{132}Sn. The results were obtained using SLy4, UNEDF1, SeaLL1, SkI2, and SkI3 parameter sets.

LED states of ^{90}Zr, we obtained LED isospin splitting, where the lower LED mode exhibits large ISD and small IVD strengths, while the higher LED mode shows the opposite. Furthermore, the transition densities of the lower and higher LED modes can take pure IS and pure IV characteristics due to the similar proton and neutron shell structures. On the other hand, in the $N \gg Z$ nuclei, the isospin characteristics of the LED modes mix due to the difference between proton and neutron shell structures near

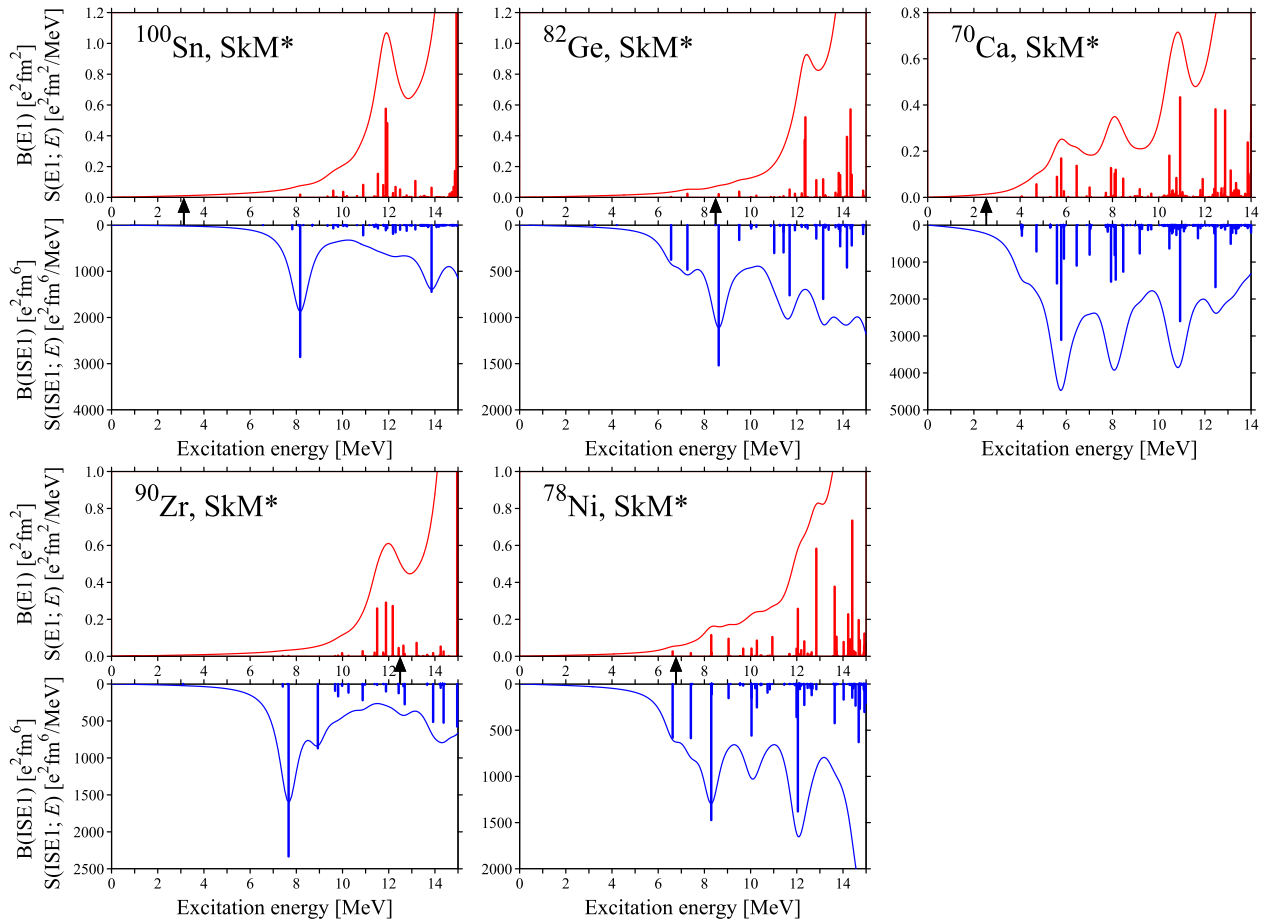

FIGURE 7
$E1$ strengths in $N = 50$ isotones, ^{100}Sn, ^{90}Zr, ^{82}Ge, ^{78}Ni, and ^{70}Ca, with the SkM* interaction. For ^{90}Zr, the figure shows the same results in Figures 2A, B.

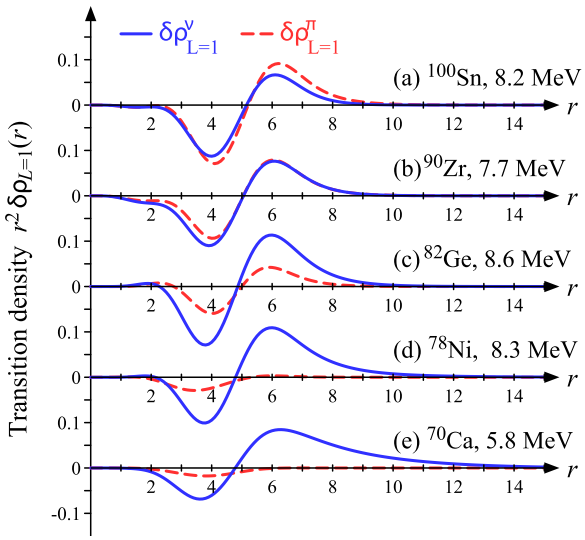

FIGURE 8
Transition densities of lower LED modes, **(A)** at 8.2 MeV in ^{100}Sn, **(B)** 7.7 MeV in ^{90}Zr, **(C)** 8.6 MeV in ^{82}Ge, **(D)** 8.3 MeV in ^{78}Ni, and **(E)** 5.8 MeV in ^{70}Ca.

the Fermi levels. This is a general property, irrespective of the used interactions.

Here, we show the transition of LED isospin splitting in $N = 50$ isotones from $N = Z$ to $N \gg Z$. Figure 7 shows the $E1$ strengths calculated with the SkM* interaction in $N = 50$ isotones, ^{100}Sn, ^{90}Zr, ^{82}Ge, ^{78}Ni, and ^{70}Ca. Interestingly, the lowest ISD mode on the proton-drip-line nucleus ^{100}Sn is essentially the same as that of the stable nucleus ^{90}Zr, as well as with its higher LED mode at 12 MeV. The transition densities of the lower LED modes for $N = 50$ isotones are shown in Figure 8, and the higher LED modes, in Figure 9. Table 3 shows the excitation energies of lower and higher LED modes and $I_{\rm iss}$s. From the viewpoints of the strengths and $I_{\rm iss}$s, the $E1$ states of ^{100}Sn, ^{90}Zr, and ^{82}Ge have the characteristic of LED isospin splitting, which is also shown in their transition densities from Figures 8, 9. The higher LED has out-of-phase two-bump transition densities regarding the fragmentation of the GDR for ^{100}Sn, ^{90}Zr, and ^{82}Ge in Figure 9. However, a small mixing of IS and IV characteristics is seen in the transition densities of the LED states in ^{82}Ge [Figures 8C, 9C]. $\delta\rho^{\pi}$ and $\delta\rho^{\nu}$ have different behaviors inside the nucleus ($r \lesssim 5$ fm). Considering ^{78}Ni, the $E1$ transition strengths at 8.3 MeV seem to have the IS dominant characteristic and its transition density and $I_{\rm iss}$ indicate the IS + IV characteristic, like the case of ^{132}Sn. The higher LED mode at 12.4 MeV has

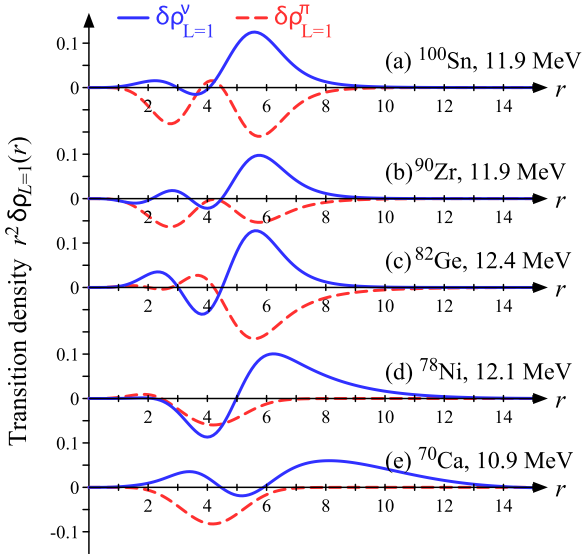

FIGURE 9
Transition densities of higher LED modes, **(A)** at 11.9 MeV in ^{100}Sn, **(B)** 11.9 MeV in ^{90}Zr, **(C)** 12.4 MeV in ^{82}Ge, **(D)** 12.1 MeV in ^{78}Ni, and **(E)** 10.9 MeV in ^{70}Ca.

TABLE 3 I_{iss} of lower and higher LED modes for $N = 50$ isotones: Excitation energy (MeV) and I_{iss} of the lower LED mode and of the higher LED mode, for each isotone.

	Lower LED E	I_{iss}	Higher LED E	I_{iss}
^{100}Sn	8.2	0.074	11.9	0.900
^{90}Zr	7.7	0.030	11.9	0.856
^{82}Ge	8.6	0.166	12.4	0.918
^{78}Ni	8.3	0.330	12.1	0.517
^{70}Ca	5.8	0.289	10.9	0.432

both large ISD and IVD strengths, but this is the neutron emission mode from the $g_{9/2}$ orbit to the continuum, which has a long tail of neutron transition density. For the LED modes of ^{70}Ca, the ISD and IVD strength distributions are similar. The lower LED at 5.8 MeV, which is composed mainly of the neutron excitation from $1f_{5/2}$ to the resonant $2d_{3/2}$ orbit, has $I_{iss} \sim 0.5$, indicating the IS + IV characteristic, while the higher LED at 10.9 MeV keeps the IV characteristic ($I_{iss} = 0.86$).

As one approaches from $N = Z$ nuclei to $N \gg Z$ nuclei, the characteristic of the LED modes changes from the pure IS or pure IV characteristic to the IS + IV characteristic, although many of the higher LED modes in $N \gg Z$ drip-line nuclei are neutron emission modes.

3.4 ISD strength and the slope parameter L

We investigate the relation between the low-energy $E1$ strengths in ^{132}Sn and the slope parameter L of EOS. The LED has attracted much attention because the LED observables strongly correlate with L [38, 39, 40]. However, the value of L has not yet been completely determined. The candidates observable have been suggested to access and determine the value of L. They are the summation of LED strength $\sum B(E1)$, the LED cross section σ_{LED}, and the LED dipole polarizability α_{LED}.

$$\sigma_{LED} = \frac{16\pi^3 e^2}{9\hbar c}\int_0^{E_{dip}} dE \quad E \quad S(E1,E),$$

$$\alpha_{LED} = \frac{8\pi e^2}{9}\int_0^{E_{dip}} dE \quad \frac{S(E1,E)}{E},$$

where E_{dip} is defined as the energy corresponding to the minimum of the strengths $S(E1;E)$ and $S(ISE1;E)$ that exist between the LED peak and the GDR on each nucleus. The upper limit of the summation of LED strength is also E_{dip}. The E_{dip} values for IVD and ISD of ^{132}Sn were all within 10 ± 1 MeV, as shown in Figure 6. Although the values depend on the smearing parameter γ, they hardly change in the range $\gamma = 0.4 - 0.6$ MeV. Table 4 lists the L values and the calculated LED observables, σ_{LED}, α_{LED}, and $\sum B(E1)$, sorted by the value of L. In this work, we add the summation of low-energy compressional ISD strength $\sum B(ISE1)$ to the candidates.

Table 4 shows linear relations between $E1$ strength observables and values of L in the Skyrme parameter sets, excluding minimal EDF SeaLL1. The linear correlations between σ_{LED}, α_{LED}, and $\sum B(E1)$ and L can be confirmed, although the linearity deviates locally. However, the sequence of L values and $\sum B(ISE1)$ calculated with Skyrme interactions aligns in Figure 10. Its Pearson correlation coefficient is $r = 0.93$ and the standard deviation is $\sigma = 624$ [e$^2 fm^6$] in this work. More detailed data are required, but this suggests that $\sum B(ISE1)$ might also be a suitable quantity for investigating L. $\widehat{D}_{IS}$ contains r^2, so it can be expected to be an operator that probes the nuclear surface more than the IVD operator $\widehat{D}$. Therefore, the strength of the ISD of neutron-rich nuclei may be an important quantity for extracting L information.

4 Conclusion

We investigated LED isospin splitting in spherical nuclei (^{40}Ca, ^{90}Zr, ^{132}Sn, ^{208}Pb, and several $N = 50$ isotones). Using fully self-consistent HF + RPA calculations with Skyrme interactions and minimal EDF in 3D Cartesian coordinates, we analyzed the isospin splitting mechanism through IVD and ISD strength functions and transition densities, introducing the isospin structure index I_{iss} for analysis.

Their LED modes vary with excitation energy for ^{40}Ca and ^{90}Zr. Below 10 MeV, $E1$ modes show large ISD and minimal IVD strengths, with transition densities in-phase for neutrons and protons (IS characteristic, $I_{iss} \sim 0$). In contrast, higher-energy $E1$ modes exhibit out-of-phase densities (IV characteristic, $I_{iss} \sim 1$). This indicates a fundamental energy-position relation between IS and IV modes in ^{40}Ca and ^{90}Zr, as confirmed by HF + RPA calculations with various interactions.

We investigated the LED states of nuclei with more neutrons than protons, stable ^{208}Pb, and unstable ^{132}Sn. The states differ from those in nuclei with $N = Z$. In both cases, the LED modes below 9 MeV show both IS and IV characteristics, with an IS + IV mixed characteristic ($I_{iss} \sim 0.5$). This mixed characteristic is expected due to different

TABLE 4 Slope parameter L and LED observables for ^{132}Sn; σ_{LED}, α_{LED}, and the summations of IVD and ISD strength $\sum^{E_{\mathrm{dip}}} B(E1)$, $\sum^{E_{\mathrm{dip}}} B(\mathrm{IS}E1)$. The interactions are sorted by the order of L value.

Interaction	L [MeV]	σ_{LED} [mb]	α_{LED} [fm^2/MeV]	$\sum B(E1)$ [e^{2}fm^2]	$\sum B(\mathrm{IS}E1)$ [e^{2}fm^6]
SeaLL1	32.4	33.8	0.555	1.076	1.25×10^4
UNEDF1	40.0	29.0	0.574	1.012	1.03×10^4
SkM*	45.8	26.4	0.402	0.808	1.18×10^4
SLy4	45.9	17.0	0.230	0.492	1.18×10^4
SkI3	100	94.5	1.078	2.508	1.34×10^4
SkI2	104	104	1.398	2.992	1.40×10^4

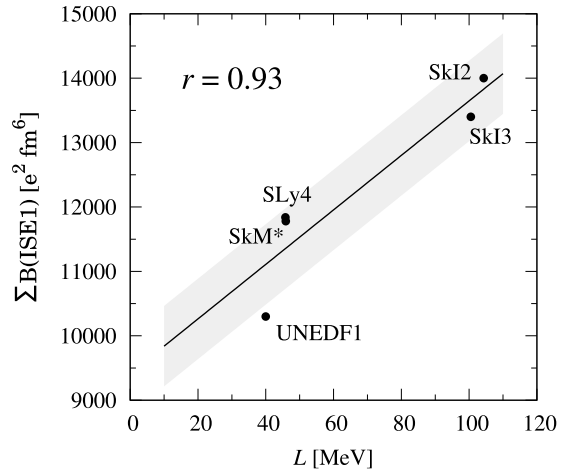

FIGURE 10
$\sum^{E_{\mathrm{dip}}} B(\mathrm{IS}E1)$ of ^{132}Sn and the parameter L calculated with Skyrme interactions. The Pearson correlation coefficient is denoted as r. The shaded area means the standard deviation σ of the linear chi-squared fit.

neutron and proton shell structures near the Fermi levels. In ^{208}Pb and ^{132}Sn, the transition densities with the IS characteristic are less favored due to the distinct shell structures. We also examined how different interactions affect the LED states of ^{132}Sn. Our HF + RPA results with SLy4 and SeaLL1 show unclear isospin splitting, whereas SkM* and UNEDF1 better reproduce the LED isospin splitting.

We calculated the LED states for spherical $N = 50$ isotones: ^{100}Sn, ^{90}Zr, ^{82}Ge, ^{78}Ni, and ^{70}Ca. We found a smooth evolution in the transition densities of E1 modes with the largest strengths below 10 MeV. In ^{100}Sn and ^{90}Zr, the $E1$ modes show pure IS or IV characteristic. In ^{82}Ge, there is a slight mixing of IS and IV due to neutron excess. For ^{78}Ni, the LED mode exhibits skin-core oscillation, while at ^{70}Ca, it shows neutron emission. As we approach the neutron drip line, the IS characteristic of the LED modes gradually shifts to a mixed IS + IV characteristic.

Finally, we showed the behaviors of the low-energy $E1$ strengths in ^{132}Sn and the slope parameter L of EOS. It was shown that the sum of the compressional ISD strengths in the low-energy region might be an important quantity for exploring the slope parameter L. This is also conjectured from the form of the ISD operator, which includes a term that probes the nuclear surface.

LED isospin splitting is characterized by the isospin (IS, IV, and IS + IV) on the dipole transition, which strongly depends on the nuclear shell structures and the neutron–proton correlation. Therefore, to measure and analyze more precisely the isospin splitting will give the fundamental knowledge of the neutron–proton correlation, and pure IS or neutron characteristic might also be extracted. In the future work, we should proceed to study isospin splitting, considering the nuclear deformation and pairing correlation theoretically.

Data availability statement

The original contributions presented in the study are included in the article/supplementary material; further inquiries can be directed to the corresponding authors.

Author contributions

TI: writing–original draft and writing–review and editing. SE: writing–original draft and writing–review and editing.

Funding

The author(s) declare financial support was received for the research, authorship, and/or publication of this article. This work was supported by the MEXT Leading Initiative for Excellent Young Researchers Grant in Japan.

Acknowledgments

The authors thank K. Hagino for the fruitful discussions.

Conflict of interest

The authors declare that the research was conducted in the absence of any commercial or financial relationships that could be construed as a potential conflict of interest.

Publisher's note

References

1. Hartmann T, Babilon M, Kamerdzhiev S, Litvinova E, Savran D, Volz S, et al. Microscopic nature of the pygmy dipole resonance: the stable Ca isotopes. *Phys Rev Lett* (2004) 93:192501. doi:10.1103/PhysRevLett.93.192501

2. Wieland O, Bracco A, Camera F, Benzoni G, Blasi N, Brambilla S, et al. Search for the Pygmy Dipole Resonance in ^{68}Ni at 600 MeV/nucleon. *Phys Rev Lett* (2009) 102:092502. doi:10.1103/PhysRevLett.102.092502

3. Schwengner R, Rusev G, Tsoneva N, Benouaret N, Beyer R, Erhard M, et al. Pygmy dipole strength in ^{90}Zr. *Phys Rev C* (2008) 78:064314. doi:10.1103/PhysRevC.78.064314

4. Iwamoto C, Utsunomiya H, Tamii A, Akimune H, Nakada H, Shima T, et al. Separation of pygmy dipole and M1 resonance in ^{90}Zr by a high-resolution inelastic proton scattering near 0°. *Phys Rev Lett* (2012) 108:262501. doi:10.1103/PhysRevLett.108.262501

5. Adrich P, Klimkiewicz A, Fallot M, Boretzky K, Aumann T, Cortina-Gil D, et al. Evidence for pygmy and giant dipole resonances in ^{130}Sn and ^{132}Sn. *Phys Rev Lett* (2005) 95:132501. doi:10.1103/PhysRevLett.95.132501

6. Tamii A, Poltoratska I, von Neumann-Cosel P, Fujita Y, Adachi T, Bertulani CA, et al. Complete electric dipole response and the neutron skin in 208Pb. *Phys Rev Lett* (2011) 107:062502. doi:10.1103/PhysRevLett.107.062502

7. Ebata S, Nakatsukasa T, Inakura T, Yoshida K, Hashimoto Y, Yabana K. Canonical-basis time-dependent Hartree-Fock-Bogoliubov theory and linear-response calculations. *Phys Rev C* (2010) 82:034306. doi:10.1103/physrevc.82.034306

8. Inakura T, Nakatsukasa T, Yabana K. Emergence of pygmy dipole resonances: magic numbers and neutron skins. *Phys Rev C* (2011) 84:021302(R). doi:10.1103/physrevc.84.021302

9. Ebata S, Nakatsukasa T, Inakura T. Systematic investigation of low-lying dipole modes using the canonical-basis time-dependent Hartree-Fock-Bogoliubov theory. *Phys Rev.C* (2014) 90:024303. doi:10.1103/physrevc.90.024303

10. Vretenar D, Paar N, Ring P, Lalazissis GA. Collectivity of the low-lying dipole strength in relativistic random phase approximation. *Nucl Phys A* (2001) 692:496–517. doi:10.1016/s0375-9474(01)00653-4

11. Paar N, Vretenar D, Khan E, Colò G. Exotic modes of excitation in atomic nuclei far from stability. *Rep Prog Phys* (2007) 70:691. doi:10.1088/0034-4885/70/5/R02

12. Savran D, Babilon M, van den Berg AM, Harakeh MN, Hasper J, Matic A, et al. Nature of the pygmy dipole resonance in ^{140}Ce studied in (alpha, alpha' gamma) experiments. *Phys Rev Lett* (2006) 97:172502. doi:10.1103/PhysRevLett.97.172502

13. Endres J, Savran D, van den Berg AM, Dendooven P, Fritzsche M, Harakeh MN, et al. Splitting of the pygmy dipole resonance in ^{138}Ba and ^{140}Ce observed in the (alpha, alpha' gamma) reaction. *Phys Rev C* (2009) 80:034302. doi:10.1103/PhysRevC.80.034302

14. Endres J, Litvinova E, Savran D, Butler PA, Harakeh MN, Harissopulos S, et al. Isospin character of the pygmy dipole resonance in ^{124}Sn. *Phys Rev Lett* (2010) 105:212503. doi:10.1103/PhysRevLett.105.212503

15. Roming C, Beller J, Glorius J, Isaak J, Kelley JH, Kwan E, et al. Low-lying dipole strength of the open-shell nucleus ^{94}Mo. *Phys Rev C* (2013) 88:044331. doi:10.1103/PhysRevC.88.044331

16. Derya V, Savran D, Endres J, Harakeh M, Hergert H, Kelley J, et al. Isospin properties of electric dipole excitations in 48Ca. *Phys Lett B* (2014) 730:288–92. doi:10.1016/j.physletb.2014.01.050

17. Negi D, Wiedeking M, Lanza EG, Litvinova E, Vitturi A, Bark RA, et al. Nature of low-lying electric dipole resonance excitations in ^{74}Ge. *Phys Rev C* (2016) 94:024332. doi:10.1103/PhysRevC.94.024332

18. Nakatsuka N, Baba H, Aumann T, Avigo R, Banerjee SR, Bracco A, et al. Observation of isoscalar and isovector dipole excitations in neutron-rich ^{20}O. *Phys Lett B* (2017) 768:387. doi:10.1016/j.physletb.2017.03.017

19. Savran D, Derya V, Bagchi S, Endres J, Harakeh MN, Isaak J, et al. Multi-messenger investigation of the pygmy dipole resonance in ^{140}Ce. *Phys Lett B* (2018) 786:16. doi:10.1016/j.physletb.2018.09.025

20. Paar N, Niu YF, Vretenar D, Meng J. Isoscalar and isovector splitting of pygmy dipole structures. *Phys Rev Lett* (2009) 103:032502. doi:10.1103/physrevlett.103.032502

21. Papakonstantinou P, Ponomarev VY, Roth R, Wambach J. Isoscalar dipole coherence at low energies and forbidden E1 strength. *Eur Phys J A* (2011) 47:14. doi:10.1140/epja/i2011-11014-7

22. Yüksel E, Khan E, Bozkurt K. Analysis of the neutron and proton contributions to the pygmy dipole mode in doubly magic nuclei. *Nucl Phys A* (2012) 877:35–50. doi:10.1016/j.nuclphysa.2012.01.006

23. Papakonstantinou P, Hergert H, Ponomarev VY, Roth R. Low-energy dipole strength and the critical case of 48Ca. *Phys Lett B* (2014) 709:270–5. doi:10.1016/j.physletb.2012.02.024

24. Vretenar D, Niu YF, Paar N, Meng J. Low-energy isovector and isoscalar dipole response in neutron-rich nuclei. *Phys Rev C* (2012) 85:044317. doi:10.1103/physrevc.85.044317

25. Nakada H, Inakura T, Sawai H. Crossover from skin mode to proton-neutron mode inE1excitations of neutron-rich nuclei. *Phys Rev C* (2013) 87:034302. doi:10.1103/physrevc.87.034302

26. Papakonstantinou P, Hergert H, Ponomarev VY, Roth R. Low-energy electric dipole response of Sn isotopes. *Phys Rev C* (2014) 89:034306. doi:10.1103/physrevc.89.034306

27. Lanza EG, Vitturi A, Litvinova E, Savran D. Dipole excitations via isoscalar probes: the splitting of the pygmy dipole resonance in124Sn. *Phys Rev C* (2014) 89:041601. doi:10.1103/physrevc.89.041601

28. Knapp F, Lo Iudice N, Veselý P, Andreozzi F, De Gregorio G, Porrino A. Dipole response inSn132within a self-consistent multiphonon approach. *Phys Rev C* (2014) 90:014310. doi:10.1103/physrevc.90.014310

29. Papakonstantinou P, Hergert H, Roth R. Isoscalar and neutron modes in theE1spectra of Ni isotopes and the relevance of shell effects and the continuum. *Phys Rev C* (2015) 92:034311. doi:10.1103/physrevc.92.034311

30. Hamamoto I, Sagawa H. Interplay between isoscalar and isovector correlations in neutron-rich nuclei. *Phys Rev C* (2017) 96:064312. doi:10.1103/physrevc.96.064312

31. Inakura T, Togano Y. Skyrme random-phase approximation analysis of low-energy dipole states in oxygen isotopes. *Phys Rev C* (2018) 97:054330. doi:10.1103/physrevc.97.054330

32. Inakura T, Imagawa H, Hashimoto Y, Mizutori S, Yamagami M, Matsuyanagi K. Mixed representation RPA calculation for octupole excitations on superdeformed states in the 40Ca and neutron-rich sulfur regions. *Nucl Phys A* (2006) 768:61–79. doi:10.1016/j.nuclphysa.2006.01.008

33. Bulgac A, Forbes MM, Jin S, Perez RN, Schunck N. Minimal nuclear energy density functional. *Phys Rev C* (2018) 97:044313. doi:10.1103/physrevc.97.044313

34. Bartel J, Quentin P, Brack M, Guet C, Håkansson HB. Towards a better parametrisation of Skyrme-like effective forces: a critical study of the SkM force. *Nucl Phys A* (1982) 386:79–100. doi:10.1016/0375-9474(82)90403-1

35. Chabanat E, Bonche P, Heenen P, Meyer J, Schaeffer R. A skyrme parametrization from subnuclear to neutron star densities part II. Nuclei far from stabilities *Nucl Phys A* (1998) 635:231. doi:10.1016/S0375-9474(98)00180-8

36. Kortelainen M, McDonnell J, Nazarewicz W, Reinhard P-G, Sarich J, Schunck N, et al. Nuclear energy density optimization: large deformations. *Phys Rev C* (2012) 85:024304. doi:10.1103/physrevc.85.024304

37. Reinhard P-G, Flocard H. Nuclear effective forces and isotope shifts. *Nucl Phys A* (1995) 584:467–88. doi:10.1016/0375-9474(94)00770-n

38. Carbone A, Col ò G, Bracco A, Cao L-G, Bortignon PF, Camera F, et al. Constraints on the symmetry energy and neutron skins from pygmy resonances in ^{68}Ni and ^{132}Sn. *Phys Rev C* (2010) 81:041301(R). doi:10.1103/PhysRevC.81.041301

39. Reinhard P-G, Nazarewicz W. Information content of a new observable: the case of the nuclear neutron skin. *Phys Rev C* (2010) 81:051303. doi:10.1103/physrevc.81.051303

40. Rossi DM, Adrich P, Aksouh F, Alvarez-Pol H, Aumann T, Benlliure J, et al. Measurement of the dipole polarizability of the unstable neutron-rich nucleus ^{68}Ni. *Phys Rev Lett* (2013) 111:242503. doi:10.1103/PhysRevLett.111.242503